International Journal of Mining Science and Technology 32 (2022) 237–245

Contents lists available at ScienceDirect

International Journal of Mining Science and Technology

journal homepage: www.elsevier.com/locate/ijmst

Limit analysis for the seismic stability of three-dimensional rock slopes using the generalized Hoek-Brown criterion

A. Karrech [a,*], X. Dong [a], M. Elchalakani [a], H. Basarir [b], M.A. Shahin [c], K. Regenauer-Lieb [d]

[a] School of Engineering, University of Western Australia, Crawley, WA 6009, Australia
[b] Department of Geoscience and Petroleum, Norwegian University of Science and Technology, Trondheim 7031, Norway
[c] School of Civil and Mechanical Engineering, Curtin University, Perth 6102, Australia
[d] School of Minerals and Energy Resources Engineering, UNSW, Sydney, NSW 2052, Australia

ARTICLE INFO

Article history:
Received 19 October 2020
Received in revised form 8 August 2021
Accepted 12 October 2021
Available online 22 October 2021

Keywords:
Three-dimensional slope
Seismic stability
Generalized Hoek-Brown criterion
Open pit

ABSTRACT

The parameters that influence slope stability and their criteria of failure are fairly understood but over-conservative design approaches are often preferred, which can result in excessive overburden removal that may jeopardize profitability in the context of open pit mining. Numerical methods such as finite element and discrete element modelling are instrumental to identify specific zones of stability, but they remain approximate and do not pinpoint the critical factors that influence stability without extensive parametric studies. A large number of degrees of freedom and input parameters may make the outcome of numerical modelling insufficient compared to analytical solutions. Existing analytical approaches have not tackled the stability of slopes using non-linear plasticity criteria and three-dimensional failure mechanisms. This paper bridges this gap by using the yield design theory and the Hoek-Brown criterion. Moreover, the proposed model includes the effect of seismic forces, which are not always taken into account in slope stability analyses. The results are presented in the form of rigorous mathematical expressions and stability charts involving the loading conditions and the rock mass properties emanating from the plasticity criterion.

1. Introduction

Slope stability is indispensable in surface mining and various geotechnical engineering applications [1–3]. Unlike service problems where the prediction of stresses/deformations around tunnels, excavation and open pits are predicted using linear elastic and/or elastic–plastic behavior, slope design deals with the condition of ultimate failure where perfect plasticity applies. There are essentially four approaches of slope stability modelling, namely the limit equilibrium method (LEM) [4–6], limit analysis method (LAM) [7–15], and computational mechanics methods (CMMs) [16–18]. LEM is a popular approach to analyze slopes both in two- and three-dimensional spaces by creating simplified failure mechanisms that make it possible to obtain safety factors based on simple equations of statics. LAM develops and applies approaches that use the conservation of energy to derive upper and lower bounds of collapse loads in engineering materials and structures. Those upper and lower bounds are also known as the kinematic and static limits [12] or plastic limit theorems [19]. The concept of collapse was defined by Drucker et al. as the "conditions for which plastic flow would occur under constant load if the accompanying change in geometry of the structure or body were disregarded", which is consistent with the fact that slope stability deals with the condition of ultimate failure. This paper focus on a sub-category of LAM, which known as the yield design theory (YDT) that shares many attributes with LAM except that it uses the duality between failure criteria and their support functions (also called π-functions) in predicting the upper (kinematic) bound [20]. The common point between LEM and LAM is the use of simple perfect plasticity (without hardening) and postulated failure mechanisms. CMMs are approximate predictive approaches based on forward numerical modelling. CMMs include the finite element method, finite difference method, discrete element modelling, and discontinuous deformation analysis, which proved to be instrumental to simulate geo-materials and geo-structures [21–28]. It is noted that many limit analysis solutions (e.g., [18]) use the finite element approach to find either the kinematically admissible velocity field or statically admissible stress field, but this does not make them CMM solutions, because they are still based on the theorems of limit analysis (LAM).

* Corresponding author.
E-mail address: ali.karrech@uwa.edu.au (A. Karrech).

https://doi.org/10.1016/j.ijmst.2021.10.005
2095-2686/

In recent years, new non-linear criteria of plasticity have attracted considerable interest as they overcome the limitations of classic linear criteria such as Mohr-Coulomb, Tresca or quadratic criteria such as Drucker-Prager and von Mises. For example, it has been indicated that the criterion of Mohr-Coulomb is insufficient to describe the behavior of rocks [29], because it overlooks the influence of loading history on the friction and the non-linear relation between stress components on the yield envelope. The more practical criterion of proved to be popular among the rock mechanics community [30]. This empirical criterion of Hoek-Brown assumes isotropic behavior and applies to intact and weathered/fractured rocks [31].

In recent years, the generalized Hoek-Brown (GHB) criterion has attracted an extensive research interest. For instance, Deng [32] investigated the stability of rock slopes using GHB by taking into account the coupling between shear dilatancy and strain softening. In addition, Liu et al. [33] studied the stability of slopes using the finite element limit equilibrium method and GHB rather than Mohr-Coulomb as accustomed. Similarly, Wei et al. [34] used the strength reduction method along with GHB to predict the optimal set of parameters triggering rock failure. Three dimensional slopes have also been studied using GHB [35,36]. The work of Xu and Yang [36] is particularly relevant to the current paper as they used Michalowski's 3D failure mechanism [5] along with GHB. However, their LAM application used the strength reduction method along with strong assumptions leading to a factor of safety that does not explicitly depend on the GHB parameters.

The generalized version of this criterion is used in this paper for slope stability analysis. Table 1 summarizes the key LEM, LAM, YDT and CMMs contributions to solving slope stability problems and indicates that most of the existing research is limited to 2D spaces and linear plasticity criteria (Mohr-Coulomb). A careful survey of the literature indicates that non-linear criteria of plasticity such as the Hoek-Brown criterion have not been used yet to solve 3D slope stability problems. Therefore, this paper fills out this gap and investigates the behavior of 3D slopes using the generalized Hoek-Brown criterion, based on LAM. In addition, this paper takes into account–in a simplistic way–the influence of earthquakes on the stability of slopes, which is often ignored in existing formulations.

2. Mathematical formulation

2.1. Kinematic approach of YDT

In this paragraph, we consider a 3D slope subjected to various external forces including gravity and seismic actions. To investigate the slope stability, it is convenient to use the principle of virtual power, which can be written:

$$\underbrace{\int_\Omega \boldsymbol{f}\cdot\boldsymbol{v}\mathrm{d}\Omega+\int_\Gamma \boldsymbol{t}\cdot\boldsymbol{v}\mathrm{d}\Gamma+\sum_i \boldsymbol{q}(\boldsymbol{x}_i)\cdot\boldsymbol{v}(\boldsymbol{x}_i)}_{\text{Virtual power of external forces},\mathbf{P}_e(\boldsymbol{v})} - \underbrace{\left(\int_\Omega \boldsymbol{\sigma}:\boldsymbol{d}\mathrm{d}\Omega+\int_{\Gamma_v}[|\boldsymbol{v}|]\cdot\boldsymbol{\sigma}\cdot\boldsymbol{n}\mathrm{d}\Gamma\right)}_{\text{Virtual power of internal forces, }\mathbf{P}_i(\boldsymbol{v})} = \underbrace{\int_\Omega \rho\boldsymbol{a}\cdot\boldsymbol{v}\mathrm{d}\Omega}_{\text{Virtual power of inertia forces, }\mathbf{P}_a(\boldsymbol{v})} \quad (1)$$

where $\boldsymbol{f}$ is a body force acting within the domain Ω; $\boldsymbol{v}$ a kinematically admissible virtual velocity which is a small, continuously differentiable velocity that satisfies the boundary conditions; $\boldsymbol{t}$ the traction force acting on the surface Γ of the composite; $\boldsymbol{q}(\boldsymbol{x}_i)$ the i^{th} concentrated force applied at the point $\boldsymbol{x}_i$; $\boldsymbol{\sigma}$ Cauchy's stress tensor; $\boldsymbol{d}$ the strain rate tensor (the symmetric part of the gradient of the virtual velocity); $[|\boldsymbol{v}|]$ the jump of velocity on the discontinuity surface Γ_v having a normal $\boldsymbol{n}$; ρ the density; and $\boldsymbol{a}$ the acceleration. The acceleration term in Eq. (1) is important because earthquakes can cause slope instability by generating inertial forces. The simplest approach to model seismic slope stability is the pseudo-static method that consists of replacing the potential inertia forces generated from ground accelerations by the horizontal and vertical static seismic forces [37]. These seismic forces are represented by horizontal and vertical forces that are proportional to the external forces acting on the rock mass with proportionality coefficients K_h and K_v, respectively. In this study, we assume that K_v is negligible unless otherwise specified, which is a commonly adopted hypothesis [14,38]. For simplification, we also consider gravity as the body force and ignore concentrated and surface forces. Hence the principle of virtual power can be rewritten as:

$$\int_\Omega (\boldsymbol{f}+K_h\|\boldsymbol{f}\|\boldsymbol{e}_h)\cdot\boldsymbol{v}\mathrm{d}\Omega=\int_\Omega \boldsymbol{\sigma}:\boldsymbol{d}\mathrm{d}\Omega+\int_{\Gamma_v}[|\boldsymbol{v}|]\cdot\boldsymbol{\sigma}\cdot\boldsymbol{n}\mathrm{d}\Gamma \quad (2)$$

where $\boldsymbol{e}_h$ is a horizontal direction. In both Eqs. (1) and (2), Cauchy stress should not exceed an elasticity envelope, $\psi(\boldsymbol{\sigma})$, that can be identified experimentally. This reflects the material's capacity of resistance that is limited by ψ at every stress state $\boldsymbol{\sigma}$. Based on this concept, the yield design theory Salençon introduced the following expressions known as π-functions [12]:

$$\begin{cases}\Pi(\boldsymbol{d})=\sup\{\boldsymbol{\sigma}:\boldsymbol{d}|\boldsymbol{\sigma}\in\psi\}\\ \Pi([|\boldsymbol{v}|],\boldsymbol{n})=\sup\{[|\boldsymbol{v}|]\cdot\boldsymbol{\sigma}\cdot\boldsymbol{n}|\boldsymbol{\sigma}\in\psi\}\end{cases} \quad (3)$$

Combining Eqs. (2) and (3) leads to the following inequality:

Table 1
Summary of literature survey on the multi-dimensional modelling of slope stability using linear and non-linear criteria and various theories.

References		Plasticity criterion		Methods			
		Mohr Coulomb	Hoek-Brown	LAM	LEM	YDT	CMMs
2D	Bishop [4]	√			√		
	Chen [7]	√		√			
	Salençon [12]	√				√	
	Michalowski [5]	√			√		
	Collins et al. [8]		√	√			
	Yu et al. [6]	√		√	√		
	Yang et al. [9]		√	√			
	Saada et al. [13]		√			√	
	Griffiths & Lane [16]	√					√
	Zheng et al. [17]		√				√
	Ukritchon & Keawsawasvong [18]	√		√			
	Belghali & Saada [14]		√			√	
3D	de Buhan & Garnier [15]	√				√	
	Michalowski and Drescher [10]	√		√			
	Xu & Yang [11]	√		√			
	Current work		√			√	

$$\underbrace{\int_\Omega (\boldsymbol{f}+K_h\|\boldsymbol{f}\|\boldsymbol{e}_h)\cdot\boldsymbol{v}\mathrm{d}\Omega}_{\text{Modified power of external forces, } \boldsymbol{P}_{me}(\boldsymbol{v})} \leqslant \underbrace{\int_\Omega \Pi(\boldsymbol{d})\mathrm{d}\Omega+\int_{\Gamma_v}\Pi([|\boldsymbol{v}|],\boldsymbol{n})\mathrm{d}\Gamma}_{\text{Maxiumum resisting power, } \boldsymbol{P}_{mr}(\boldsymbol{v})} \quad (4)$$

The expression $\boldsymbol{P}_{me}(\boldsymbol{v}) \leq \boldsymbol{P}_{mr}(\boldsymbol{v})$ is known as the kinematic approach or the upper bound of limit analysis. This method is effective when the virtual velocity $\boldsymbol{v}$ is kinematically admissible and the modified power of external forces $\boldsymbol{P}_{me}(\boldsymbol{v})$ is finite.

2.2. Support function of the Hoek-Brown plasticity envelope

To calculate the maximum resisting power $\boldsymbol{P}_{mr}$, it is important to identify the π-function of interest. In the current study, we consider a homogeneous isotropic behaviour and focus on the generalised Hoek-Brown criterion of plasticity [30,31]. The corresponding envelope of elasticity reads $\psi=\{\boldsymbol{\sigma}|f(\boldsymbol{\sigma}) \leq 0\}$, where the criterion is defined as follows:

$$\frac{\sigma_1-\sigma_3}{\sigma_c}=\left(-\frac{m\sigma_1}{\sigma_c}+s\right)^n \quad (5)$$

where σ_1 is the major principal stress; σ_3 the minor principal stress; σ_c the uniaxial compressive strength; and the convention of positive stress in tension is adopted. The parameters of the Hoek-Brown expression Eq. (5) depend on the geological strength index (GSI) as follows:

$$\begin{cases} \frac{m}{m_i}=\exp\left(\frac{GSI-100}{28-14D}\right) \\ s=\exp\left(\frac{GSI-100}{9-3D}\right) \\ n=\frac{1}{2}+\frac{1}{6}\left[\exp\left(-\frac{GSI}{15}\right)-\exp\left(-\frac{20}{3}\right)\right] \end{cases} \quad (6)$$

where m_i is a material property of intact rocks; and D a disturbance factor that varies from 0.0 to 1.0 corresponding to undisturbed in-situ rock masses to very disturbed rock masses, respectively. Note that m_i is roughly related to the ratio between compressive and tensile strengths and GSI describes structural blockiness and the conditions of joint systems as perceived at the surface of a rock mass. The Hoek-Brown criterion was proposed to fit the results of several triaxial tests conducted on a wide range of rocks; it is expressed in terms of major and minor principal stresses. It was criticized for ignoring the intermediate stress, which proved to influence rock strength [39–41]. As is, the criterion is insufficient to describe the three-dimensional constitutive behavior and flow of geomaterials through numerical integration. To overcome these limitations, generalized models were proposed in terms of stress invariants [42,43]. In general, these modified criteria were expressed in terms of first Cauchy stress invariant, I_1, second deviatoric stress invariant, J_2, third deviatoric stress invariant, J_3, and Lode angle, θ_d, defined by:

$$\begin{cases} I_1=\mathrm{tr}\boldsymbol{\sigma}=\sigma_1+\sigma_2+\sigma_3 \\ J_2=\frac{\boldsymbol{s}:\boldsymbol{s}}{2}=\frac{(\sigma_1-\sigma_2)^2+(\sigma_2-\sigma_3)^2+(\sigma_3-\sigma_1)^2}{6} \\ J_3=\det(\boldsymbol{s})=\mathrm{tr}(\boldsymbol{s}:\boldsymbol{s}:\boldsymbol{s}) \\ \theta_d=\frac{1}{3}\arcsin\left(-\frac{3\sqrt{3}}{2}\frac{J_3}{\sqrt{J_2^3}}\right)=\arcsin\frac{1}{\sqrt{3}}\frac{2\sigma_2-\sigma_1-\sigma_3}{\sigma_1-\sigma_3} \end{cases} \quad (7)$$

where $\boldsymbol{s}=\boldsymbol{\sigma}-(I_1/3)\cdot\boldsymbol{1}$ is the deviatoric stress and $\boldsymbol{1}$ is the unit tensor [44]. The Lode angle varies from $-\pi/6$ and $\pi/6$. The three-dimensional version of Hoek-Brown's criterion can be expressed as:

$$f(\boldsymbol{\sigma})=2\cos\theta_d\sqrt{J_2} - \sigma_c\left\{s+\frac{m}{\sigma_c}\left(-\frac{I_1}{3}+\left[\sin\theta_d-\sqrt{3}\cos\theta_d\right]\sqrt{\frac{J_2}{3}}\right)\right\}^n \quad (8)$$

The triaxial tests are usually conducted either under triaxial compression ($\sigma_1=\sigma_2>\sigma_3$) or triaxial extension ($\sigma_3=\sigma_2<\sigma_1$) corresponding to $\theta_d=\pi/6$ and $-\pi/6$, respectively. A smooth transition between the triaxial compression and triaxial extension conditions is possible by using an elliptic Lode dependence to describe the failure of rocks under multi-axial loading states [45].

The support π-functions Eq. (3) of Hoek-Brown's Eq. (8) can be calculated by maximizing $\boldsymbol{\sigma}:\boldsymbol{d}$ and/or $[|\boldsymbol{v}|]\cdot\boldsymbol{\sigma}\cdot\boldsymbol{n}$ depending on the mode of dissipation. Based on the concept of plastic collapse explained in the introduction [19], it is convenient to assume that the significant permanent displacements (and deformations) occur at the interfaces of the failure mechanism. Therefore, $\Pi([|\boldsymbol{v}|],\boldsymbol{n})$ governs the dissipation process. Knowing the stress tensor, this expression can be obtained by decomposing the jump of velocity $[|\boldsymbol{v}|]$ on the discontinuity surface Γ_v into v_n, v_t and v_s where the subscripts "n", "t" and "s" denote the normal and tangential directions, respectively. At the discontinuity surface, the strain rate tensor $\boldsymbol{d}$ takes the form:

$$\frac{1}{2}([|\boldsymbol{v}|]\otimes\boldsymbol{n}+\boldsymbol{n}\otimes[|\boldsymbol{v}|])=\begin{pmatrix} v_n & \frac{v_t}{2} & \frac{v_s}{2} \\ \frac{v_t}{2} & 0 & 0 \\ \frac{v_s}{2} & 0 & 0 \end{pmatrix} \quad (9)$$

which results in the following expression:

$$\Pi([|\boldsymbol{v}|],\boldsymbol{n})=\sigma_n v_n+\tau v_t \quad (10)$$

Given that v_s is zero because the problem is symmetric. It can be verified that the expression of $\Pi(|[\boldsymbol{v}|],\boldsymbol{n})$ verifies all the properties of support functions since it is positive (given that stress and strain are co-axial), homogeneous of degree one (it can be easily verified that $\Pi(a[|\boldsymbol{v}|],\boldsymbol{n})=a\Pi([|\boldsymbol{v}|],\boldsymbol{n})$ for all $a>0$), and convex (it can be verified that $\Pi(a[|\boldsymbol{v_1}|]+(1-a)[|\boldsymbol{v_2}|],\boldsymbol{n})=a\Pi([|\boldsymbol{v_1}|],\boldsymbol{n})+(1-a)\Pi([|\boldsymbol{v_2}|],\boldsymbol{n})$ for all a in the interval [0,1]).

2.3. Failure mechanism

We investigate the slope depicted in Fig. 1, characterized by a height H and an inclination angle β ranging from 0° to 90°. The slope is subjected to the body force of gravity and seismic inertial forces. The failure mechanism considered in this study is a three-dimensional curvilinear cone (horn shape) inspired by [10] and containing a planar insert. The velocity in 3D curvilinear cone is expressed as follows:

$$v=r\omega \quad (11)$$

where r is the radius of curvature; and ω the angular velocity around the axis $\boldsymbol{e}_3$ passing through O. The failure mechanism is uniquely determined knowing the crest and toe angles θ_A and θ_C, respectively, as well as the log-spiral arcs AC and $A'C'$, which are both characterised by an angle ϕ and focus O, as shown in Fig. 1a. The lower and upper lo-spirals describing AC and $A'C'$ are:

$$\begin{cases} r=r_A\mathrm{e}^{(\theta-\theta_A)\tan\phi} \\ r'=r'_A\mathrm{e}^{(\theta-\theta_A)\tan\phi} \end{cases} \quad (12)$$

where r_A and r'_A are the polar radii to the points A and A'.

2.4. Power of external loading and resisting power

The rate of infinitesimal power done by the gravity and inertial forces within small element $d\Omega$ belonging to the horn shaped failure mechanism (Fig. 1) is as follows:

$$\gamma v(\cos\theta+K_h\sin\theta)\mathrm{d}\Omega=\gamma v(\cos\theta+K_h\sin\theta)\mathrm{d}x\mathrm{d}y(r_m+y)\mathrm{d}\theta \quad (13)$$

where $\gamma=\rho g$ is the specific weight; g the gravity constant; $r_m=0.5(r+r')$ the distance between point O and the axis of the failure mechanism; and $R=0.5(r-r')$ the radius of the cross section as indicated in Fig. 1a. The velocity at the surface of discontinuity is $v=\omega(r_m+y)$. Note that the difference between the expressions obtained in this study and the expression of external work rate obtained by

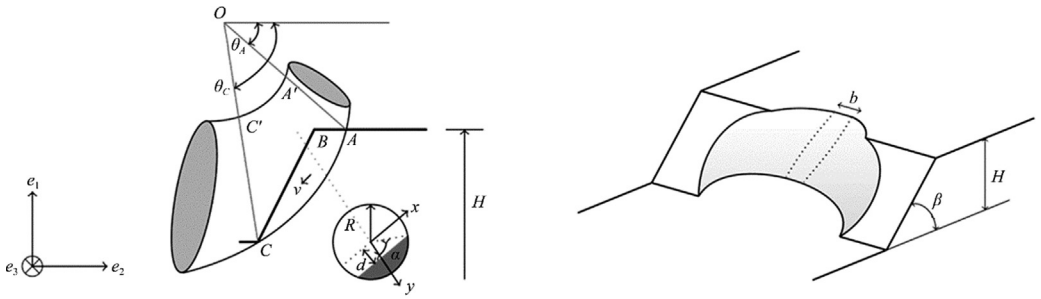

(a) 'Hornshape' surface without planar insert (b) Slope where a planer insert is included

Fig. 1. Schematic representation of the three-dimensional slope failure mechanism.

[11] is due to the effect of seismic forces. Integrating Eq. (13) leads to:

$$\begin{aligned}&2\omega\gamma\int_{\theta_A}^{\theta_B}\int_0^{x_1}\int_{d_1}^{\sqrt{R^2-x^2}}(\cos\theta+K_h\sin\theta)\mathrm{d}x\mathrm{d}y(r_m+y)^2\mathrm{d}\theta+\\&2\omega\gamma\int_{\theta_B}^{\theta_C}\int_0^{x_2}\int_{d_2}^{\sqrt{R^2-x^2}}(\cos\theta+K_h\sin\theta)\mathrm{d}x\mathrm{d}y(r_m+y)^2\mathrm{d}\theta\end{aligned}\tag{14}$$

where $x_i^2=R^2-d_i^2$ $(i=1,2)$ as indicated in the circular section cut depicted in Fig. 1a. Eq. (14) can be simplified to obtain the following expression:

$$\begin{aligned}&2\omega\gamma r_A^4\left\{\int_{\theta_A}^{\theta_B}w_1(\theta)(\cos\theta+K_h\sin\theta)\mathrm{d}\theta+\int_{\theta_B}^{\theta_C}w_2(\theta)(\cos\theta+K_h\sin\theta)\mathrm{d}\theta\right\}\\&\qquad=2\omega\gamma r_A^4(f_0+K_hf_0^s)\end{aligned}\tag{15}$$

where the dimensionless constants f_0 and f_0^s are expressed in more detail in Appendix B. When a planar insert is considered, the corresponding rate of work done by gravity and inertial forces is:

$$\omega\gamma br_A^3\{f_1-f_2-f_3+K_h(f_1^s-f_2^s-f_3^s)\}\tag{16}$$

where the dimensionless terms f_1, f_2, and f_3 have been derived by [7] and the dimensionless terms f_1^s, f_2^s and f_3^s have been derived by [46]. Note that both references treated two dimensional slopes of unit thickness, hence the width constant b that appears in our expression. These expressions are listed in Appendix B for convenience. Therefore, the left-hand side (LHS) of Eq. (4) representing the external work of the gravity and seismic forces can be obtained as follows:

$$\mathrm{P}_e=\omega\gamma r_A^4\left[2(f_0+K_hf_0^s)+\frac{b}{r_A}\{f_1-f_2-f_3+K_h(f_1^s-f_2^s-f_3^s)\}\right]\tag{17}$$

Combining Eq. (A.4) with the expression of $\Pi([|\boldsymbol{v}|],\boldsymbol{n})$ in Eq. (10), we obtain:

$$\Pi([|\boldsymbol{v}|],\boldsymbol{n})=\left\{\left(n^{\frac{n}{1-n}}-n^{\frac{1}{1-n}}\right)\left(\frac{1-\sin\phi_t}{2\sin\phi_t}\right)^{\frac{1}{1-n}}m^{\frac{n}{1-n}}+\frac{s}{m}\right\}\sigma_c\tan\phi_t v_t\tag{18}$$

In addition, substituting for the support function Eq. (18) into Eq. (4), we obtain the expression of maximum resisting power P_{mr}, as follows:

$$\begin{aligned}\mathrm{P}_{mr}=&2\omega\Sigma_c\sigma_c\left\{\int_{\theta_A}^{\theta_B}\int_0^{\alpha_1}R(r_m+R\cos\alpha)^2\mathrm{d}\alpha\mathrm{d}\theta\right.\\&\left.+\int_{\theta_B}^{\theta_C}\int_0^{\alpha_2}R(r_m+R\cos\alpha)^2\mathrm{d}\alpha\mathrm{d}\theta\right\}\\&+\omega br_A^2\Sigma_c\sigma_c\int_{\theta_A}^{\theta_C}\mathrm{e}^{2(\theta-\theta_A)\tan\phi}\mathrm{d}\theta\end{aligned}\tag{19}$$

where $\alpha_i=\arccos(d_i/R)(i=1,2)$, and,

$$\Sigma_c=\left\{\left(n^{\frac{n}{1-n}}-n^{\frac{1}{1-n}}\right)\left(\frac{(1-\sin\phi_t)}{2\sin\phi_t}\right)^{\frac{1}{1-n}}m^{\frac{n}{1-n}}+\frac{s}{m}\right\}\tan\phi_t$$

Integrating Eq. (19) shows that:

$$\mathrm{P}_{mr}=\omega\Sigma_c\sigma_c r_A^3\left\{g_0+\frac{b}{2r_A}\cot\phi\left(\mathrm{e}^{2(\theta_C-\theta_A)\tan\phi}-1\right)\right\}\tag{20}$$

where g_0 is a dimensionless parameter that is detailed in Appendix B.

2.5. Safety factor

The factor of safety (or safety factor) is used to quantify a margin of safety based on intrinsic strength against prescribed loading conditions. Usually, the safety factor is computed in terms of stresses (ratio of yield stress over working stress). In this paper, we use an energy-based ratio because energy encompasses stress and strain which makes it physically more meaningful. The factor of safety is defined as:

$$FoS=\frac{\mathrm{P}_{mr}}{\mathrm{P}_e}\tag{21}$$

By definition, the *FoS* should be greater or equal to 1, which is a necessary condition of slope stability. The definition of *FoS* requires that P_e be strictly positive. Combining Eqs. (17), (20), and (21) shows that

$$FoS=\frac{\frac{\Sigma_c H}{r_A}\left\{g_0+\frac{b}{2r_A}\cot\phi\left(\mathrm{e}^{2(\theta_C-\theta_A)\tan\phi}-1\right)\right\}}{\frac{\gamma H}{\sigma_c}\cdot\left(2(f_0+K_hf_0^s)+\frac{b}{r_A}\{f_1-f_2-f_3+K_h(f_1^s-f_2^s-f_3^s)\}\right)}\tag{22}$$

The term $\eta=\gamma H/\sigma_c$ that appears in Eq. (22) is known as the stability factor, which is a key slope design parameter [18]. Apart from η, *FoS* depends on the slope geometry (H, β, b, r_A, r_A', θ_A and, θ_C) and the material properties (σ_c, m, m_i, s, n, and, *GSI*). The critical safety factor can be obtained by minimising *FoS* with respect to the problem variables r_A, θ_A, θ_C, and ϕ, while taking into account the constraints $0<\phi<\pi/2$, $0<\theta_A<\theta_C<\pi-\beta$, $\sin(\beta+\theta_A)-\mathrm{e}^{(\theta_A-\theta_C)\tan\phi}\cdot\sin(\beta+\theta_A)>0$, and $r_A>0$.

3. Results and discussion

3.1. Model verification

To verify the proposed model, we first considered the models proposed by [8,9] who focused on the behavior of two-dimensional slopes obeying the Hoek-Brown criterion. Both research teams described the stability of slopes in the absence of seismic forces using a static stability factor. The stability factor corresponding to the linear yield criterion of Mohr-Coulomb is $N_L=-\gamma H_c/c$ where H_c is the critical slope height and c is cohesion. The non-linear stability factor corresponding to the original Hoek-Brown criterion has been defined as $N_N=\gamma H_c/(s^{0.5}\sigma_c)$. Collins et al.

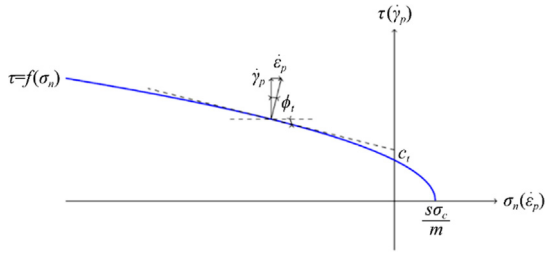

Fig. 2. Mohr plane representation of Hoek-Brown's criterion.

[8] related the linear stability factor N_L obtained based on the Mohr-Coulomb criterion to the non-linear stability factor N_N obtained based on the original Hoek-Brown criterion using a relationship of the form $N_N = N_L(\phi_t)\cdot c_t(\phi_t)/(s^{0.5}\sigma_c)$ where $c_t(\phi_t)$ is the intercept of the tangent to the yield function as shown in Fig. 2.

Yang et al. [9] proposed to use the same expression for the generalized Hoek-Brown criterion. In this study, we use the concept safety factor (Eq. (22)) rather than stability factor to assess stability. As discussed by Belghali & Saada [14], the two factors are equivalent in estimating the critical slope conditions when $FoS = 1$ in Eq. (22). Hence, to compare our results to those of Collins et al. [8] and Yang et al. [9], we use the following non-linear stability factor:

$$N_N = \frac{\frac{\Sigma_c H}{r_A\sqrt{s}}\left\{g_0 + \frac{b}{2r_A}\cot\phi\left(e^{2(\theta_C-\theta_A)\tan\phi}-1\right)\right\}}{\left(2\left(f_0+K_h f_0^s\right)+\frac{b}{r_A}\left\{f_1-f_2-f_3+K_h\left(f_1^s-f_2^s-f_3^s\right)\right\}\right)} \tag{23}$$

which we minimize with respect to θ_A, θ_C, and ϕ. Since this analysis is based on a kinematic upper bound that leads to a critical slope factor, N_N, expressed by Eq. (23) should be minimized to identify the failure mechanism parameters. The minimization procedure has been implemented in python using the Nelder-Mead optimization method, a downhill simplex approach that is available in the scipy module of python. It can be seen that our 3D expression generalizes the expression obtained by Belghali & Saada [14] in 2D. This can be verified easily by tending b/r_A to infinite to recover the planar discussed by Collins et al. [8], Yang et al. [9], and Belghali & Saada [14] under various conditions. As such, Table 2 shows a comparison between our results and previous calculations. It can be seen that our approach is in close agreement with the result of Collins et al. [8], Yang et al. [9] when we consider $b \gg r_A$. It is important to compare Eq. (23) with the results of Xu and Yang [36]; it can be seen that our expression is explicitly dependent on Σ_c, which is a function of m, n, s, and σ_c that appear in the generalized Hoek-Brown criterion. This is direct consequence of using an energetic approach to express the maximum resisting power via the π-function Eq. (18). In the absence of a model that uses a 3D failure mechanism and Hoek-Brown's criterion, we compared our results to those of Michalowski & Drescher [10] and Xu & Yang [11] who both used the linear Mohr-Coulomb criterion as a plasticity envelope. This has been achieved by varying b/r_A to progressively move away from the 2D case presented in Table 2. Fig. 3 shows that when B/H increases (i.e. $b \gg r_A$), the stability factor tends asymptotically to the values presented in Table 2. However, when B/H is small (around unity), the stability factor increases hyperbolically in agreement with the results of Michalowski & Drescher [10] and Xu & Yang [11]. As indicated by Michalowski & Drescher [10], admissible mechanisms passing through the toe cannot be achieved for very small B/H, which is physically meaningful since a minimum size is required to move materials from the crest across the toe.

By way of summary to this subsection, we transformed the safety factor expressed by Eq. (22) into a stability factor expressed by Eq. (23) by postulating that the slope is critical when FoS is equal to unity as suggested by Belghali & Saada [14] who used the same approach in 2D. Our results are in good agreement with the results Collins et al. [8] Yang et al. [9] as shown in Table 1. In addition, our model is in agreement with the models Michalowski & Drescher [10] and Xu & Yang [11] in terms of behavior of stability factor with respect to the mechanism's width as shown in Fig. 3, despite the difference in magnitude which is attributed to the difference in failure criterion. In fact, the magnitudes obtained in this study are valid because the curves tend asymptotically to the values listed in Table 2. After this verification of the model's validity and accuracy, we will discuss its implications in the next subsection.

3.2. Design charts

The geometry of the problem has a considerable effect on the slope stability; as shown in Fig. 3, the stability factor increases as the ration B/H decreases. This means that two-dimensional slope stability models can be over-conservative and may result in unnecessary waste removal in the context of surface mining. In this section, we consider the particular case of $B/H = 2.5$ since the planar insert has to be decided by the designer. In other words, the geologist or the engineer would estimate the insert width based on geological features or field experience, knowing that larger features result in smaller stability factors (i.e. entail higher risks). The geometrical attributes of the failure mechanisms are all obtained by minimization as discussed in Subsection 4.1. Hence, the remaining variables of the problem that influence the slope stability are essentially rock properties, seismic forces, slope angle, which are investigated in this subsection.

3.3. Effects of rock properties

The rock properties investigated in this paper are encompassed by the Hoek-Brown criterion, given that the yield design theory focuses on plastic collapse. As can be seen in Eq. (6), the parame-

Table 2
Comparison between the stability factors obtained for $b \gg r_A$ and the solutions of Collins et al. [8] and Yang et al. [9] when $K_h = 0$ and $n = 0.5$.

β	Reference	Parameters s, m				
		s=1.0 m=15.7	s=0.1 m=6.638	s=0.0044 m=1.7117	s=0.0001 m=0.2822	s=0.00001 m=0.0786
60°	Yang et al. [9]	8.78	10.97	13.57	14.07	12.61
	Collins et al. [8]	8.80	10.97	13.89	13.89	12.38
	Current work	8.94	11.10	13.54	13.77	12.18
50°	Yang et al. [9]	15.32	19.95	15.34	26.37	23.26
	Collins et al. [8]	15.36	19.93	25.18	26.00	22.89
	Current work	15.75	20.33	25.54	25.95	22.67
45°	Yang et al. [9]	20.22	26.60	34.00	35.41	31.28
	Collins et al. [8]	20.28	26.64	33.89	35.01	30.73
	Current work	20.86	27.20	34.24	34.94	30.43

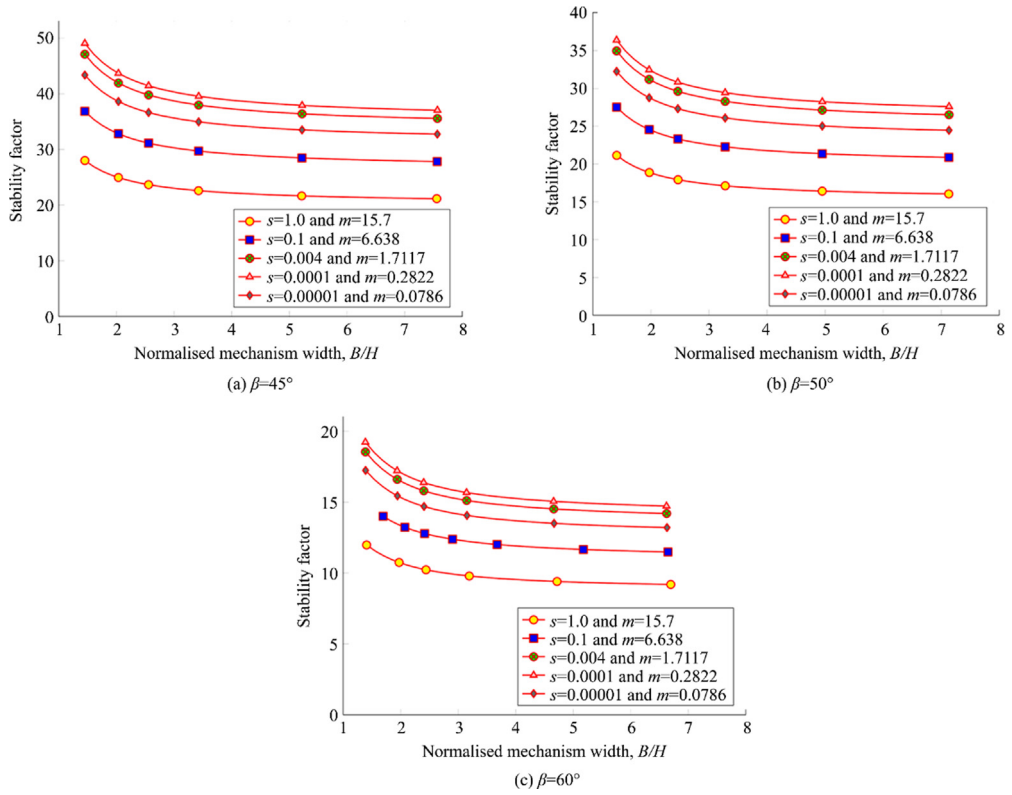

Fig. 3. Model verification – slope stability factor for various geometries and material properties.

ters of the Hoek-Brown criterion m, s, and n depend on the material constant for intact rocks, m_i, the geological strength index, *GSI*, and the disturbance factor, D. Note that the uniaxial compressive strength, σ_c, is not included in the expression of slope stability factor as shown in Eq. (23). However, it can be used to estimate the critical slope height as explained in the subsequent paragraphs. Assuming undisturbed rocks, the coefficient D is considered zero in this section, without loss of generality. The left-hand side curves of Fig. 4 depict the variation of the non-linear stability factor, N_N with the Hoek-Brown variable, m_i. As indicated by Zhang [47], m_i depends on the rock type and texture. For example, it tends to be higher in igneous rocks than in sedimentary and metamorphic rocks and increases as the grain size increases. Our result indicate that the stability factor increases systematically when m_i increases, irrespective of other properties or geometrical considerations. The right-hand side curves of Fig. 4 represent the variation of the non-linear stability factor, N_N, with the geological strength index, *GSI*. The geological strength was introduced by Hoek [31] to replace Bieniawski's rock mass rating (RMR) classification; it reflects the structural blockiness of rocks and their joint conditions. The figure indicates that N_N increases then decreases with respect to *GSI*, suggesting that the optimum stability occurs between 30 and 50, irrespective of other material properties. The figure also indicates that the optimum *GSI* increases as the slope angle increases. While this behavior may appear counterintuitive, it is mathematically justifiable given that N_N is proportional to $\Sigma_c/(s^{0.5})$, which depends non-linearly on *GSI*.

3.4. Effects of seismic forces

Seismic forces are often ignored in slope stability models, despite the significance of seismic activities in most mining sites (including in ears with low risk of earthquakes). For example, close to blast zones, inertial forces can be significant and may affect the local rock mass stability. For simplification, we limited this analysis to horizontal seismic forces, but vertical components can be implemented following a similar procedure. Seismicity is dealt with using static equivalent forces represented by the coefficient K_h as shown in Eq. (2). Fig. 4 shows the results obtained for K_h = 0.1, 0.2 and 0.3 for various slope angles and material properties. These results show that increasing the coefficient K_h by an increment of 0.1 almost halves the stability condition at each step. This means that increasing the seismic forces systematically decreases the non-linear stability factor, which increases the risk of failure as expected.

3.5. Effect of slope angle

The slope angle strongly influences rock stability in open pits, along hill roads or even in naturally occurring geological structures. These angles are generally selected depending on the material conditions to avoid large failures and rockfalls. Slopes play various roles including the definition and protection of cut surfaces and may vary with depth as weathered rocks that are close to the surface often require shallower slope angles than rocks at depth. To simplify this analysis we considered a single slope angle, but the results can be generalized by using an inclined top surface [9,14]. As shown in Fig. 4, the non-linear stability factor decreases systematically as the slope angle increases, which confirms that steeper slopes provide lower stability. Interestingly, the left-hand side of the figure indicates that the optimum *GSI* value increases as the slope angle increases. For example, this optimum is obtained at *GSI* = 30 for β = 45° and at *GSI* = 40 for β = 70°. The maximum N_N decreases non-linearly in between.

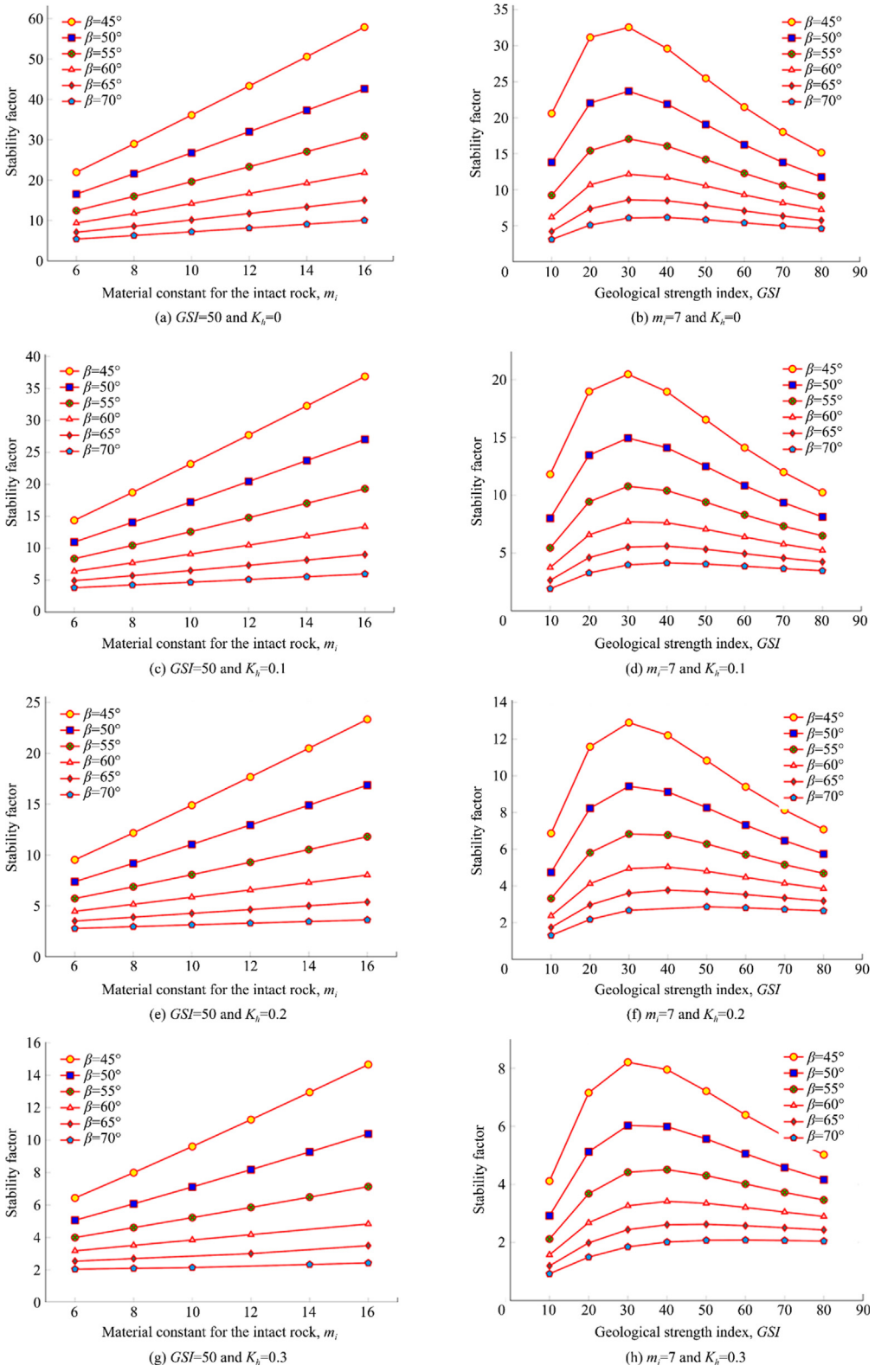

Fig. 4. Effects of Hoek-Brown parameters on the slope stability factor for various horizontal coefficients of seismic forces.

4. Conclusions

A new model that uses the non-linear plasticity criterion of Hoek-Brown, the yield design theory and a three-dimensional failure mechanism has been introduced to predict the behavior of rock mass slopes that can be encountered in mining and civil engineering applications. The proposed model takes into account the effect of seismic forces by using an equivalent static approach. By applying the principle of virtual power and maximizing dissipation, a non-linear stability factor is obtained which takes into account the parameters of the failure mechanism, geometry of the slope, the material properties, and the coefficients of seismic forces. To

eliminate the failure mechanism influence, the non-linear stability factor is minimized using the Nelder-Mead optimization method. The proposed model is verified using special cases that have been investigated previously; the results of this model showed excellent agreement with the studies used to benchmark it. Hence, the following remarks can be made:

(1) Two dimensional models are over-conservative since they under-estimate the stability factor. Using them for slope stability modelling may result in unnecessary rock waste removal in the context of surface mining that can jeopardize profitability.
(2) The slope stability improves as the Hoek-Brown coefficient m_i increases (i.e. may be interpreted as increasingly favorable compression to tension strengths) and/or the slope angle decreases (i.e. the slope becomes shallower).
(3) The optimum geological strength index ranges from 30 to 40 depending on the slope angle.
(4) Ignoring seismic forces can be misleading since the stability factor reduces when the seismic coefficient increases. Existing design methods that overlook seismic activities related to earthquakes or blasting are insufficient since they overestimate the stability factor. The model developed in this paper shows that an increment of 0.1 in the seismic coefficient almost halves the stability factor.

Appendix A. π-functions

Fig. 2 depicts the Hoek-Brown yield surface in the Mohr space (σ_n, τ). Assuming an associated flow rule, the plastic strain rate ($\dot{\varepsilon}_p, \dot{\gamma}_p$) must be normal to the yield surface as indicated in the figure and the $\dot{\varepsilon}_p$ is calculated as:

$$\dot{\varepsilon}_p = \tan\phi_t \dot{\gamma}_p \tag{A.1}$$

where $\tan\phi_t = \partial\tau/\partial\sigma_n$. A tangential line to the yield surface in Fig. 2 indicates that $\tau = c_t - \sigma_n \cdot \tan\phi_t$. According to Yang et al. [9], the pseudo-cohesion, c_t, can be expressed as follows:

$$\frac{c_t}{\sigma_c} = \frac{\cos\phi_t}{2}\left(\frac{mn(1-\sin\phi_t)}{2\sin\phi_t}\right)^{\frac{n}{1-n}} - \frac{\tan\phi_t}{m}\left(1+\frac{\sin\phi_t}{n}\right)\left(\frac{mn(1-\sin\phi_t)}{2\sin\phi_t}\right)^{\frac{1}{1-n}} + \frac{s}{m}\tan\phi_t \tag{A.2}$$

The shear and normal strain rates $\dot{\varepsilon}_p$ and $\dot{\gamma}_p$ are equal to v_t/e and v_n/e, respectively, where e is the thickness of the narrow transition area between the stable and unstable regions of the slope. The members of strain tensor are assumed uniform within this transition area, which means that thickness is as small as required. Hence, Eq. (A.1) indicates that $\delta v_n = \tan\phi_t \cdot \delta v_t$. Using the support function expressed by Eq. (10) and the above results shows that:

$$\Pi([\![\boldsymbol{v}]\!], \boldsymbol{n}) = \sigma_n v_n + \tau v_t = (\sigma_n \tan\phi_t + \tau) v_t = c_t v_t \tag{A.3}$$

The expression of the pseudo-cohesion coefficient c_t shown in Eq. (A.2) can be simplified as follows:

$$\frac{c_t}{\sigma_c} = \left(\frac{1-\sin\phi_t}{2\sin\phi_t}\right)^{\frac{1}{1-n}} m^{\frac{n}{1-n}} \tan\phi_t \left(n^{\frac{n}{1-n}} - n^{\frac{1}{1-n}}\right) + \frac{s}{m}\tan\phi_t \tag{A.4}$$

Appendix B. Dimensionless constants in the expressions of work

To define the dimensionless constants of external work and maximum resistance, we first define the following expressions:

$$\begin{cases} h_1 = \frac{r_m}{r_A} = \frac{r+r'}{2r_A} = \frac{1}{2}\left(e^{(\theta-\theta_A)\tan\phi} + \frac{r'_A}{r_A}e^{-(\theta-\theta_A)\tan\phi}\right) \\ h_2 = \frac{R}{r_A} = \frac{r-r'}{2r_A} = \frac{1}{2}\left(e^{(\theta-\theta_A)\tan\phi} - \frac{r'_A}{r_A}e^{-(\theta-\theta_A)\tan\phi}\right) \\ h_3 = \frac{d_1}{r_A} = \frac{\sin\theta_A}{\sin\theta} - \frac{r_m}{r_A} = \frac{\sin\theta_A}{\sin\theta} - h_1 \\ h_4 = \frac{d_2}{r_A} = \frac{\sin\theta_A \sin(\theta_B+\beta)}{\sin\theta_B \sin(\theta+\beta)} - h_1 \end{cases} \tag{B.1}$$

From Eq. (15), it can be seen that:

$$\begin{cases} f_0 = \int_{\theta_A}^{\theta_B} w_1(\theta)\cos\theta \mathrm{d}\theta + \int_{\theta_B}^{\theta_C} w_2(\theta)\cos\theta \mathrm{d}\theta \\ f_0^s = \int_{\theta_A}^{\theta_B} w_1(\theta)\sin\theta \mathrm{d}\theta + \int_{\theta_B}^{\theta_C} w_2(\theta)\sin\theta \mathrm{d}\theta \end{cases} \tag{B.2}$$

where,

$$w_i(\theta) = \sqrt{h_2^2 - h_{i+2}^2}\left[\frac{h_2^2 h_{i+2}}{8} - \frac{h_{i+2}^3}{4} - \frac{h_{i+2}h_1^2}{2} - \frac{2h_{i+2}^2 h_1}{3} + \frac{2h_2^2 h_1}{3}\right] + \frac{h_2^2\left(h_2^2+4h_1^2\right)}{8}\arccos\frac{h_{i+2}}{h_2}, \text{ and } i = 1 \text{ or } 2$$

The dimensionless terms in Eq. (16) are:

$$\begin{cases} f_1 = \frac{(3\tan\phi\cos\theta_C + \sin\theta_C)e^{3(\theta_C-\theta_A)\tan\phi} - (3\tan\phi\cos\theta_A + \sin\theta_A)}{3\left(1+9\tan^2\phi\right)} \\ f_2 = \zeta(2\cos\theta_A - \zeta)\sin\theta_A/6 \\ f_3 = \frac{H}{r_A}\frac{\sin(\theta_C+\beta)}{6\sin\beta}e^{(\theta_C-\theta_A)\tan\phi}\left(\cos\theta_C e^{(\theta_C-\theta_A)\tan\phi} + \cos\theta_A - \zeta\right) \\ f_1^s = \frac{(3\tan\phi\sin\theta_C - \cos\theta_C)e^{3(\theta_C-\theta_A)\tan\phi} - (3\tan\phi\sin\theta_A - \cos\theta_A)}{3\left(1+9\tan^2\phi\right)} \\ f_2^s = \zeta\sin^2\theta_A/3 \\ f_3^s = \frac{H}{r_A}\frac{\sin(\theta_C+\beta)}{6\sin\beta}e^{(\theta_C-\theta_A)\tan\phi}\left(\sin\theta_C e^{(\theta_C-\theta_A)\tan\phi} + \sin\theta_A\right) \end{cases} \tag{B.3}$$

where

$$\zeta = \frac{\sin(\theta_A+\beta) - \sin(\theta_C+\beta)e^{(\theta_C-\theta_A)\tan\phi}}{\sin\beta}$$

From Eq. (19), it can be seen that:

$$g_0 = \int_{\theta_A}^{\theta_B} w_3(\theta)\mathrm{d}\theta + \int_{\theta_B}^{\theta_C} w_4(\theta)\mathrm{d}\theta \tag{B.4}$$

where,

$$\theta_B = \arctan\frac{\sin\theta_A}{\cos\theta_A - \zeta}$$

$$w_{i+2}(\theta) = h_2\left(\left(h_2^2 + 2h_1^2\right)\alpha_i + h_2(4h_1 + h_2\cos\alpha_i)\sin\alpha_i\right), \; i = 1 \text{ or } 2,$$

and, $\alpha_i = \arccos\frac{h_{i+2}}{h_2}$.

References

[1] Obregon C, Mitri H. Probabilistic approach for open pit bench slope stability analysis – a mine case study. Int J Min Sci Technol 2019;29:629–40.
[2] McQuillan A, Canbulat I, Oh J. Methods applied in Australian industry to evaluate coal mine slope stability. Int J Min Sci Technol 2020;30:151–5.
[3] Bar N, Kostadinovski M, Tucker M, Byng G, Rachmatullah R, Maldonado A, et al. Rapid and robust slope failure appraisal using aerial photogrammetry and 3D slope stability models. Int J Min Sci Technol 2020;30:651–8.
[4] Bishop AW. The use of the slip circle in the stability analysis of slopes. Géotechnique 1955;5:7–17.
[5] Michalowski RL. Slope stability analysis: a kinematical approach. Géotechnique 1995;45(2):283–93.
[6] Yu HS, Salgado R, Sloan SW, Kim JM. Limit analysis versus limit equilibrium for slope stability. J Geotech Geoenviron Eng 1998;124:1–11.
[7] Chen WF. Limit Analysis and Soil Plasticity. Amesterdam: Elsevier; 1975.
[8] Collins IF, Gunn CIM, Pender MJ, Yan W. Slope stability analyses for materials with a non-linear failure envelope. Int J Numer Anal Meth Geomech 1988;12:533–50.
[9] Yang XL, Li L, Yin JH. Seismic and static stability analysis for rock slopes by a kinematical approach. Géotechnique 2004;54:543–9.
[10] Michalowski R, Drescher A. Three-dimensional stability of slopes and excavations. Géotechnique 2009;5:839–50.

[11] Xu JS, Yang XL. Three-dimensional stability analysis of slope in unsaturated soils considering strength nonlinearity under water drawdown. Eng Geol 2018;237:102–15.
[12] Salençon J. Calcul à la rupture et analyse limite. Paris: Presse de l'école nationale des ponts et chaussées; 1983.
[13] Saada Z, Maghous S, Garnier D. Bearing capacity of shallow foundations on rocks obeying a modified Hoek-Brown failure criterion. Comput Geotech 2008;35(2):144–54.
[14] Belghali M, Saada Z. Seismic stability analysis of rock slopes by yield design theory using the generalized Hoek-Brown criterion 2018;149.
[15] de Buhan P, Garnier D. Three dimensional bearing capacity analysis of a foundation near a slope. Soils Found 1998;38:153–63.
[16] Griffiths DV, Lane PA. Slope stability analysis by finite elements. Géotechnique 1999;49:387–403.
[17] Zheng H, Liu DF, Li CG. Slope stability analysis based on elasto-plastic finite element method. Int J Numer Meth Eng 2005;64:1871–88.
[18] Ukritchon B, Keawsawasvong S. A new design equation for drained stability of conical slopes in cohesive-frictional soils. J Rock Mech Geotech Eng 2018;10:358–66.
[19] Drucker DC, Prager W, Greenberg HJ. Extended limit design theorems for continuous media. Q Appl Math 1952;9:381–9.
[20] Prager W. Théorie générale des états limites d'équilibre. Journal de Mathématiques Pures et Appliquées 1955;9:395–406.
[21] Karrech A, Regenauer-Lieb K, Poulet T. A limit analysis approach to derive a thermodynamic damage potential for non-linear geomaterials. Phil Mag 2012;92:3439–50.
[22] Karrech A, Duhamel D, Bonnet G, Chevoir F, Roux JN, Canou J, Dupla CJ. A discrete element study of settlement in vibrated granular layers: role of contact loss and acceleration. Granular Matter 2008;10:369–75.
[23] Gaede O, Regenauer-Lieb K, Karrech A. Anisotropic damage mechanics as a novel approach to improve pre- and post-failure borehole stability analysis. Geophys J Int 2013;193:1095–109.
[24] Karrech A, Schrank C, Freij-Ayoub R, Regenauer-Lieb K. A multi-scaling approach to predict hydraulic damage of poromaterials. Int J Mech Sci 2014;78:1–7.
[25] Peters M, Veveakis M, Poulet T, Karrech A, Herwegh M, Regenauer-Lieb K. Boudinage as a material instability of elasto-visco-plastic rocks. J Struct Geol 2015;78:86–102.
[26] Karrech A, Duhamel D, Bonnet G, Roux J, Chevoir F, Canou J, Dupla J, Sab K. A computational procedure for the prediction of settlement in granular materials under cyclic loading. Comput Methods Appl Mech Eng 2007;197:80–94.
[27] Karrech A, Seibi A, Duhamel D. Finite element modelling of rate-dependent ratcheting in granular materials. Comput Geotech 2011;38:105–12.
[28] Karrech A, Schrank C, Regenauer-Lieb K. A parallel computing tool for large-scale simulation of massive fluid injection in thermo-poro-mechanical systems. Phil Mag 2015;95:3078–102.
[29] Jaeger JC. Friction of rocks and stability of rock slopes. Géotechnique 1971;21:97–134.
[30] Hoek E, Brown E. Underground Excavations in Rock. London: CRC Press; 1980.
[31] Hoek E. Strength of jointed rock masses. Géotechnique 1983;33:187–223.
[32] Deng DP. Limit equilibrium solution for the rock slope stability under the coupling effect of the shear dilatancy and strain softening. Int J Rock Mech Min Sci 2020;134:104421.
[33] Liu S, Su Z, Li M, Shao L. Slope stability analysis using elastic finite element stress fields. Eng Geol 2020;273:105673.
[34] Yuan W, Li JX, Li ZH, Wang W, Sun XY. A strength reduction method based on the Generalized Hoek-Brown (GHB) criterion for rock slope stability analysis. Comput Geotech 2020;117:103240.
[35] Li Y, Yang X. Three-dimensional Seismic Displacement Analysis of Rock Slopes based on Hoek-Brown Failure Criterion. KSCE J Civ Eng 2018;22(11):4334–44.
[36] Xu J, Yang X. Seismic stability analysis and charts of a 3D rock slope in Hoek-Brown media. Int J Rock Mech Min Sci 2018;112:64–76.
[37] Seed HB. Considerations in the earthquake-resistant design of earth and rockfill dams. Géotechnique 1979;29:215–63.
[38] Saada Z, Maghous S, Garnier D. Seismic bearing capacity of shallow foundations near rock slopes using the generalized Hoek-Brown criterion. Int J Numer Anal Meth Geomech 2011;35:724–48.
[39] Al-Ajmi AM, Zimmerman RW. Relation between the mogi and the coulomb failure criteria. Int J Rock Mech Min Sci 2005;42:431–9.
[40] Wang R, Kemeny J M. A new empirical failure criterion for rock under polyaxial compressive stresses. In: Proceeding of the 35th U.S. Symposium on Rock Mechanics (USRMS). Reno, Nevada, 1995.
[41] Colmenares LB, Zoback MD. A statistical evaluation of intact rock failure criteria constrained by polyaxial test data for five different rocks. Int J Rock Mech Min Sci 2002;39:695–729.
[42] Jaiswal A, Shrivastva BK. A generalized three-dimensional failure criterion for rock masses. J Rock Mech Geotech Eng 2012;4:333–43.
[43] Zhang Q, Zhu H, Zhang L. Modification of a generalized three-dimensional Hoek-Brown strength criterion. Int J Rock Mech Min Sci 2013;59:80–96.
[44] Jiang H. Three-dimensional failure criteria for rocks based on the Hoek-Brown criterion and a general lode dependence. Int J Geomech 2017;17:04017023.
[45] Jiang H, Yang Y. A three-dimensional Hoek-Brown failure criterion based on an elliptical Lode dependence. Int J Numer Anal Meth Geomech 2020;44:2395–411.
[46] Chang CJ, Chen WF, Yao JTP. Seismic displacements in slopes by limit analysis. J Geotech Eng 1984;110:860–74.
[47] Zhang L. A generalized three-dimensional Hoek-Brown strength criterion. Rock Mech Rock Eng 2008;41:893–915.